Optics Letters

Polarization-dependent strong coupling between surface plasmon polaritons and excitons in an organic-dye-doped nanostructure

Kun Zhang,[1] Tian-Yong Chen,[1] Wen-Bo Shi,[1] Cheng-Yao Li,[1] Ren-Hao Fan,[1] Qian-Jin Wang,[1] Ru-Wen Peng,[1,2] and Mu Wang[1,3]

[1]National Laboratory of Solid State Microstructures, School of Physics, and Collaborative Innovation Center of Advanced Microstructures, Nanjing University, Nanjing 210093, China
[2]e-mail: rwpeng@nju.edu.cn
[3]e-mail: muwang@nju.edu.cn

Received 16 May 2017; revised 19 June 2017; accepted 20 June 2017; posted 21 June 2017 (Doc. ID 295991); published 14 July 2017

In this work, we demonstrate polarization-dependent strong coupling between surface plasmon polaritons (SPPs) and excitons in the *J*-aggregates-attached aperture array. It is shown that the excitons strongly couple with the polarization-dependent SPPs, and Rabi splittings are consequently observed. As a result, the polarization-dependent polariton bands are generated in the system. Increasing the incident angle, the polaritons disperse to higher energies under transverse-electric illumination, while the polaritons disperse to lower energies under transverse-magnetic illumination. Therefore, at different polarization incidence, we experimentally achieve distinct polaritons with opposite dispersion directions. In this way, tuning the polarization of the incident light, we can excite different polaritons whose energy propagates to different directions. Furthermore, by retrieving the mixing fractions of the components in these polariton bands, we find that the dispersion properties of the polaritons are inherited from both the SPPs and the excitons. Our investigation may inspire related studies on tunable photon–exciton interactions and achieve some potential applications on active polariton devices.

OCIS codes: (240.5420) Polaritons; (250.5403) Plasmonics; (160.4890) Organic materials; (230.5440) Polarization-selective devices.

https://doi.org/10.1364/OL.42.002834

Recently, interactions between photons and excitons have attracted continuous interest, especially in the case of strong coupling. Photon–exciton strong coupling takes place when the energy exchange rate between them prevails over their damping rates, generating quasi-particles called polaritons. The two hybrid polariton bands exhibit anti-crossing behavior in *k*-space, which is the Rabi splitting, and the Rabi splitting energy is related to the photon–exciton coupling energy. Strong coupling with large coupling energy can be realized more easily when Frenkel excitons in organic semiconductors are employed because of their higher binding energy, saturation density, and oscillator strength. Such strong couplings have been demonstrated in various systems, for example, in optical cavities supporting cavity modes [1–9] and nanostructures supporting surface plasmon polaritons (SPPs) [10–24], helping to guide and manipulate polaritons at the nanoscale.

Beyond the fundamental interest, polaritons also provide the building blocks for quantum information systems [25–27], polariton condensation [28–30], and low-threshold nanolasers [31,32], offering possibilities to realize all-optical circuits and photonic quantum devices. There have already been some interesting attempts on promising applications of polaritons. For example, some researchers are approaching the quantum limit [18,21], and some are trying to introduce multimode hybrid polariton bands in one system [7–9,12,24,33]. There are also some works exploring tunable platforms to control the polaritons' behavior. On the one hand, tunable photonic nanostructures are employed, such as polarization-dependent plexcitonic crystals [15] and tunable hemispherical open-access microcavities [34]. On the other hand, tunable photon–exciton strong coupling based on an electric-sensitive transition metal dichalcogenide monolayer has been realized [33].

In this work, we offer another platform to actively tune the strong coupling between excitons and SPPs by the polarization of incident light. We attach *J*-aggregates on the top of a two-dimensional aperture array, similar to the system in Ref. [13], but we specifically set the aperture periods to be different along the two axes. Thereafter, polarization-dependent SPPs are excited in the array, and the excitons in the *J*-aggregates can strongly couple with the SPPs, resulting in polarization-dependent polaritons. Our work offers another degree of freedom to control the energy propagation of polaritons, which may inspire related studies about light–matter interactions and achieve potential applications on tunable polariton devices.

First, we adjust the geometric parameters of the two-dimensional aperture array using the commercial finite-difference time-domain (FDTD) simulation software package (Lumerical FDTD Solutions). As schematically described in Fig. 1(a), the

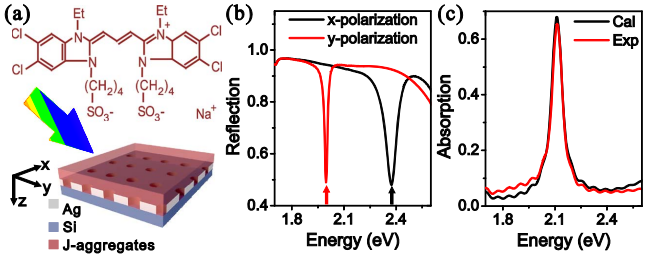

Fig. 1. (a) Schematic description of the aperture array covered by PVA film with J-aggregates; the inset gives the chemical formula of TDBC used to form J-aggregates. (b) Calculated reflection spectrum of the aperture array covered by pure PVA film under normal incidence with different polarizations. (c) Black line shows the calculated absorption spectrum of the PVA-TDBC film, fitting well with the experimental results shown by the red line.

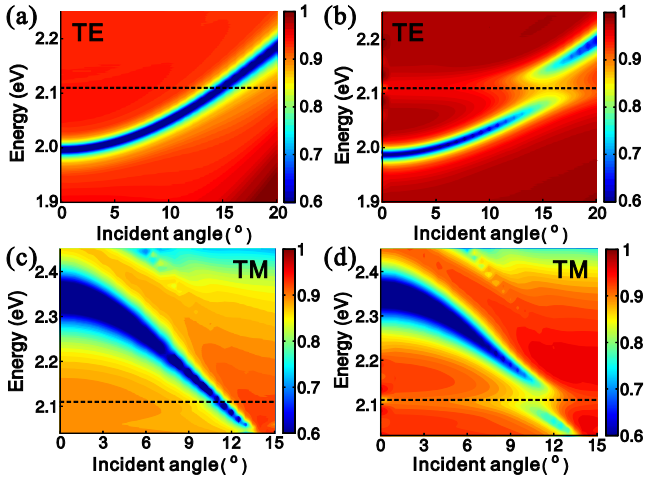

Fig. 2. (a) and (b) Show the calculated angle-resolved reflection spectra under TE illumination, (c) and (d) show those under TM illumination, where (a) and (c) correspond to the sample covered by PVA film, and (b) and (d) correspond to the one covered by PVA-TDBC film. The dashed black lines indicate the energy of excitons in the J-aggregates.

apertures are etched in a 120-nm-thick silver film on the silicon substrate. The aperture radius is $r = 40$ nm, the period in the x direction is $P_x = 295$ nm, and that in y direction is $P_y = 370$ nm. We then cover the aperture array by pure polyvinyl alcohol (PVA) film, and calculate the reflection spectrum under normal incidence. In this system, the excited SPPs satisfy $\vec{k}_{spps} = \vec{k}_0 \sin\theta + i\vec{G}_x + j\vec{G}_y$, where $\vec{k}_{spps}$ is the wave vector of SPPs, $\vec{k}_0 \sin\theta$ is the in-plane wave vector of incident light, $|\vec{G}_x| = 2\pi/P_x$ and $|\vec{G}_y| = 2\pi/P_y$ are the amplitudes of reciprocal lattice vectors, and i, j are both integers [13,35–37]. So the wavelength of the reflection dip under normal incidence follows the expression that $\lambda_{dip} = \sqrt{\varepsilon_d \varepsilon_{eff}/(\varepsilon_d + \varepsilon_{eff})}/\sqrt{i^2/P_x^2 + j^2/P_y^2}$, where ε_d and ε_{eff} are the permittivities of PVA and the structured silver film, respectively. As indicated by the arrows in Fig. 1(b), the resonant dip at 2.36 eV corresponds to SPPs excited under x polarization, and the one at 1.99 eV corresponds to SPPs excited under y polarization. As a result, different SPP modes can be excited under different polarizations.

By attaching PVA film with J-aggregates onto the aperture array to replace the pure PVA film, excitons can be introduced. In our study, we use the organic dye TDBC to form the J-aggregates, whose chemical formula is given as the inset in Fig. 1(a). To fit the permittivity of the PVA-TDBC film, we use the following single Lorentzian oscillator model [16]:

$$\varepsilon_J(\omega) = \varepsilon_\infty + \frac{f\omega_0^2}{\omega_0^2 - \omega^2 - i\gamma\omega}, \quad (1)$$

where ε_∞ is the permittivity of pure PVA film, ω_0 is the oscillator frequency, γ is the damping constant, and f is the oscillator strength. To make a best fit to the experimentally measured results, we find the fitted parameters to be $\varepsilon_\infty = 2.56$, $\omega_0 = 3.2 \times 10^{15}$ rad/s, $\gamma = 4 \times 10^{13}$ rad/s, and $f = 0.003$. Employing these fitted parameters, the calculated absorption spectrum is shown by the black line in Fig. 1(c), fitting well with the experimental data [shown by the red line in Fig. 1(c)], indicating that the excitons' energy is around 2.11 eV.

Sweeping the incident angles under different polarizations, the angle-resolved reflection spectra correspond to the dispersion map of the SPP modes. In our study, the incident plane is fixed to be the x-z plane. In this way, transverse-electric (TE) illumination corresponds to the incident light keeping its electric field polarized along the y axis, while transverse-magnetic (TM) illumination corresponds to the incident light with electric field polarized along the x axis.

Under TE illumination, the calculated angle-resolved reflection spectra of the aperture array covered by pure PVA film are drawn in Fig. 2(a). As the incident angle increases, the SPP mode disperses to higher energies. At about 15°, the energy of the reflection dip goes across the energy of the excitons, indicating a strong coupling around this angle. Such a photon–exciton strong coupling can be seen clearly in Fig. 2(b), which shows the calculated angle-resolved reflection spectra of the aperture array covered by PVA-TDBC film. There is an obvious anti-crossing behavior around 2.11 eV, which means two polariton bands emerging because of the strong coupling. The two polariton bands both disperse from lower energies to higher energies as the incident angle increases, similar to the SPP mode. Under TM illumination, the calculated angle-resolved reflection spectra are shown in Fig. 2(c). As the incident angle increases, the SPP mode disperses to lower energies. At about 11°, the energy of the reflection dip intersects with the excitons' energy, and strong coupling around this angle is clearly observed in Fig. 2(d). Contrary to the TE illumination, the two polariton bands here both disperse from higher energies to lower energies, in accordance with the behavior of the SPP mode.

The SPPs' Bragg diffraction in the periodic aperture array yields a folding of the SPPs' dispersion curve [13], which leads to the different dispersion directions shown in Figs. 2(a) and 2(c). As a result, we can totally get two pairs of polariton bands with different dispersion directions in this J-aggregates-covered aperture array, and their presence can be tuned by the polarization of incident light.

Employing the geometric parameters in simulation, we fabricate the sample experimentally. The silver film is deposited on the silicon substrate via magnetron sputtering, and then the aperture array is etched in it by focus-ion-beam milling (FIB, Helios Nanolab 600i). The scanning electronic microscope (SEM) image of the sample is shown in Fig. 3(a). Covering

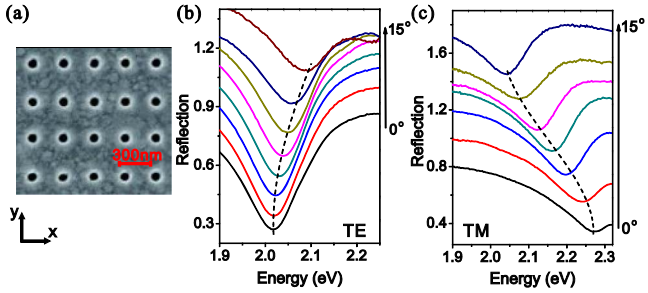

Fig. 3. (a) SEM photo of the aperture array; (b) and (c) respectively show the measured angle-resolved reflection spectra of the aperture array covered by pure PVA film under TE and TM illumination with a vertical offset for different incident angles, and the black dashed lines trace their dispersions.

the sample with pure PVA film, we then measure the angle-resolved reflection spectra by sweeping the incident angles. Under normal incidence, the SPP mode excited by x polarization is around 2.02 eV, while that excited by y polarization is around 2.27 eV. These energies have a little difference from the calculated data, which may be caused by the deviations in fabrication process. Under TE illumination, as the results displayed in Fig. 3(b) show, the SPP mode disperses from lower energies to higher energies, corresponding with the simulation results in Fig. 2(a). While under TM illumination, as shown in Fig. 3(c), the dispersion direction of the SPPs reverses, and they disperse from higher energies to lower energies, matching well with the data in Fig. 2(c).

To demonstrate the polarization-dependent SPPs–exciton strong coupling, we cover the aperture array with PVA-TDBC film, and then measure its angle-resolved reflection spectra under different polarizations. Under TE illumination, we can see the two polariton bands as traced by the black dashed lines in Fig. 4(a). Both the lower polariton band (TE-LPB) and the upper polariton band (TE-UPB) disperse from lower energies to higher energies as the incident angle increases. Here, we enlarge the spectra above 2.11 eV in order to see the TE-UPB more clearly. Although the energy of the reflection dip at 15° is lower than 2.11 eV, there is still effective overlap between the SPP mode and the excitons because these two modes are broad enough, leading to the strong coupling between them. Under TM illumination, on the contrary, the TM-LPB and TM-UPB traced by the black dashed lines both disperse from higher energies to lower energies as the incident angle increases. Converting these data to two-dimensional angle-resolved reflection spectra, as shown in Figs. 4(c) and 4(d), we can see the obvious anti-crossing phenomena around the intersecting incident angles, like the behaviors respectively described in Figs. 2(b) and 2(d).

The strong coupling between the SPPs and excitons can be expressed by the coupled harmonic oscillator equations as

$$\begin{pmatrix} E_{\mathrm{spp}}^{\mathrm{TE(TM)}} & \hbar\Omega^{\mathrm{TE(TM)}}/2 \\ \hbar\Omega^{\mathrm{TE(TM)}}/2 & E_{ex} \end{pmatrix} \begin{pmatrix} \alpha_{\mathrm{spp}}^{\mathrm{TE(TM)}} \\ \alpha_{ex}^{\mathrm{TE(TM)}} \end{pmatrix} = E_p^{\mathrm{TE(TM)}}(\theta) \begin{pmatrix} \alpha_{\mathrm{spp}}^{\mathrm{TE(TM)}} \\ \alpha_{ex}^{\mathrm{TE(TM)}} \end{pmatrix}, \quad (2)$$

where $E_{\mathrm{spp}}^{\mathrm{TE}}$ (or $E_{\mathrm{spp}}^{\mathrm{TM}}$) represents the energy of the SPP mode excited under TE (or TM) illumination, E_{ex} represents the exciton energy, $\hbar\Omega^{\mathrm{TE(TM)}}$ is the coupling energy between the corresponding SPP mode and excitons, $E_p^{\mathrm{TE}}(\theta)$ [or $E_p^{\mathrm{TM}}(\theta)$] represents the energy of the emerged polariton mode, and the mixing fractions $\alpha_{\mathrm{spp}}^{\mathrm{TE}}$ (or $\alpha_{\mathrm{spp}}^{\mathrm{TM}}$) and α_{ex} are the relative weightings of SPPs and excitons in the polariton bands. From the angle-resolved reflection spectra in Figs. 4(c) and 4(d), we can find that the coupling energy under TE illumination is $\hbar\Omega^{\mathrm{TE}} = 200$ meV, and that under TM illumination is $\hbar\Omega^{\mathrm{TM}} = 250$ meV. Due to the imperfection of the fabricated sample and the parameter deviations between experiments and simulations, the measured Rabi splitting energies are larger than those in simulation. Using the measured Rabi splitting energies, we can calculate the energies of the polariton bands employing Eq. (2); the results are drawn by the white dashed lines in Figs. 4(c) and 4(d), fitting well with the experimental data.

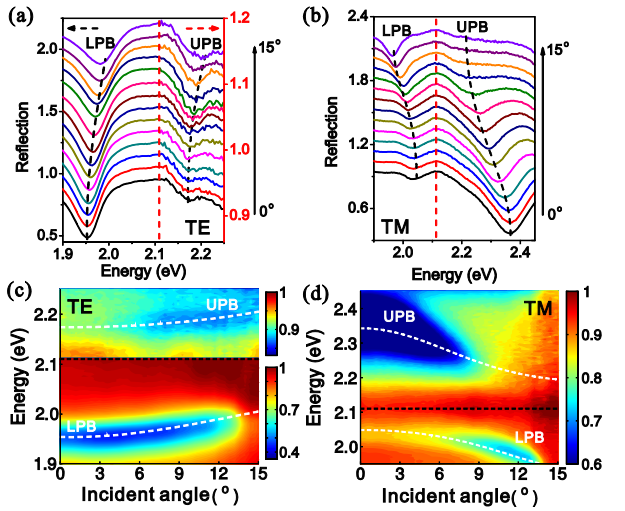

Fig. 4. Measured reflection spectra of the sample covered by PVA-TDBC film under (a) TE and (b) TM illumination with a vertical offset for different incident angles. The black dashed lines trace the polariton bands, and the red dashed lines indicate the exciton energy; (c) and (d) respectively show the angle-resolved reflection spectra corresponding to the results in (a) and (b). The white dashed lines indicate the fitted results, and the black dashed lines indicate the excitons' energy.

Besides fitting the polariton bands, we can also retrieve the mixing fractions by using the experimental data to solve Eq. (2). It is apparent, as displayed in Fig. 5, that every polariton mode is a hybrid state consisting of SPP components and exciton components. With the increase of incident angles, as shown in Fig. 5(a), the mixing fraction of SPPs in TE-UPB increases and that of excitons decreases; on the other hand, the mixing fraction of SPPs in TE-LPB decreases and that of excitons

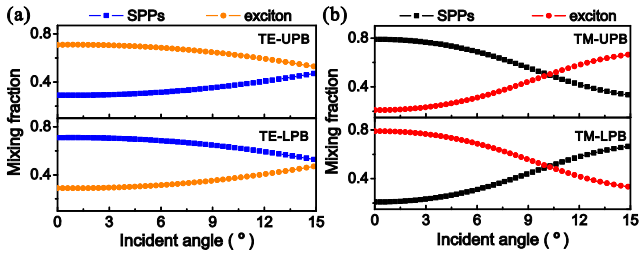

Fig. 5. Mixing fractions of the SPPs and excitons in the polariton bands under (a) TE and (b) TM illumination.

increases. On the contrary, under TM illumination, it is obvious in Fig. 5(b) that the variation trends of the mixing fractions in TM-UPB are similar to those in TE-LPB, while the mixing fractions in TM-LPB change in the similar trends of those in TE-UPB. These results can perfectly explain the dispersion behaviors of the polariton bands. As the excitons are nondispersive, all the polariton bands disperse in the same directions as the SPPs but disperse more gently. Therefore, the variation trends of the relative weightings of the SPPs and excitons in the polariton bands help to understand their optical behaviors.

As we know, the group velocity of light can be expressed as $v_g = \mathrm{d}\omega/\mathrm{d}k$, representing the propagation velocity of energy. Thereafter, the tangent line's slope of every polariton band in Figs. 4(c) and 4(d) is related to the group velocity of the polaritons. In this way, the x components of the polaritons' group velocities under TE illumination are positive, i.e., $v_{g\_x}^{\mathrm{TE}} > 0$, while those of the polariton bands under TM illumination are negative, i.e., $v_{g\_x}^{\mathrm{TM}} < 0$, meaning that their energy propagation directions along the x axis are opposite to each other. In this system, by tuning the polarization of the incident light, we can get polaritons propagating to different directions, offering another degree of freedom to control the polaritons' energy propagation.

In summary, we have experimentally fabricated a two-dimensional aperture array in silver film to support polarization-dependent SPPs. Covering this array with J-aggregates, excitons are easily introduced. Thereafter, polarization-dependent strong couplings between SPPs and excitons are realized. Under TE illumination, the polariton bands both disperse to the higher energies as the incident angles increase. Contrarily, the polariton bands both disperse to lower energies under TM illumination. As a result, by tuning the polarization of incident light, we have achieved different polariton bands with reverse dispersion, i.e., this platform supports different polaritons whose energies propagate to different directions. Using the coupled harmonic oscillator equations, we have fit the polariton bands and retrieved the mixing fractions of SPPs and excitons in every band. The dispersion behaviors of the polariton bands are explained by the variation trends of the relative weightings of SPPs and excitons. Our approach has offered a way to tune the polariton dispersions by the incident light polarization, showing another degree of freedom to control the polariton propagation, which may inspire related studies on tunable photon–exciton interactions and achieve potential applications on tunable polariton devices.

Funding. Ministry of Science and Technology of the People's Republic of China (MOST) (2017YFA0303700); National Natural Science Foundation of China (NSFC) (11634005, 61475070, 11474157, 11674155, 11621091); "333 Project" from Jiangsu Province (BRA2016350).

REFERENCES

1. D. G. Lidzey, D. D. C. Bradley, M. S. Skolnick, T. Virgili, S. Walker, and D. M. Whittaker, Nature **395**, 53 (1998).
2. D. G. Lidzey, D. D. C. Bradley, T. Virgili, A. Armitage, and M. S. Skolnick, Phys. Rev. Lett. **82**, 3316 (1999).
3. R. J. Holmes and S. R. Forrest, Phys. Rev. Lett. **93**, 186404 (2004).
4. S. Hayashi, Y. Ishigaki, and M. Fujii, Phys. Rev. B **86**, 045408 (2012).
5. S. Pirotta, M. Patrini, M. Liscidini, M. Galli, G. Dacarro, G. Canazza, G. Guizzetti, D. Comoretto, and D. Bajoni, Appl. Phys. Lett. **104**, 051111 (2014).
6. D. Ballarini, M. D. Giorgi, S. Gambino, G. Lerario, M. Mazzeo, A. Genco, G. Accorsi, C. Giansante, S. Colella, S. D'Agostino, P. Cazzato, D. Sanvitto, and G. Gigli, Adv. Opt. Mater. **2**, 1076 (2014).
7. D. M. Coles, N. Somaschi, P. Michetti, C. Clark, P. G. Lagoudakis, P. G. Savvidis, and D. G. Lidzey, Nat. Mater. **13**, 712 (2014).
8. D. M. Coles and D. G. Lidzey, Appl. Phys. Lett. **104**, 191108 (2014).
9. K. Zhang, Y. Xu, T.-Y. Chen, H. Jing, W.-B. Shi, B. Xiong, R.-W. Peng, and M. Wang, Opt. Lett. **41**, 5740 (2016).
10. J. Bellessa, C. Bonnand, J. C. Plenet, and J. Mugnier, Phys. Rev. Lett. **93**, 036404 (2004).
11. N. T. Fofang, T.-H. Park, O. Neumann, N. A. Mirin, P. Nordlander, and N. J. Halas, Nano Lett. **8**, 3481 (2008).
12. T. K. Hakala, J. J. Toppari, A. Kuzyk, M. Pettersson, H. Tikkanen, H. Kunttu, and P. Törmä, Phys. Rev. Lett. **103**, 053602 (2009).
13. J. Dintinger, S. Klein, F. Bustos, W. L. Barnes, and T. W. Ebbesen, Phys. Rev. B **71**, 035424 (2005).
14. W. Wang, P. Vasa, R. Pomraenke, R. Vogelgesang, A. D. Sio, E. Sommer, M. Maiuri, C. Manzoni, G. Cerullo, and C. Lienau, ACS Nano **8**, 1056 (2014).
15. E. Karademir, S. Balci, C. Kocabas, and A. Aydinli, Opt. Express **22**, 21912 (2014).
16. E. Eizner and T. Ellenbogen, Appl. Phys. Lett. **104**, 223301 (2014).
17. P. Vasa, W. Wang, R. Pomraenke, M. Maiuri, C. Manzoni, G. Cerullo, and C. Lienau, Phys. Rev. Lett. **114**, 036802 (2015).
18. G. Zengin, M. Wersall, S. Nilsson, T. J. Antosiewicz, M. Kall, and T. Shegai, Phys. Rev. Lett. **114**, 157401 (2015).
19. E. Eizner, O. Avayu, R. Ditcovski, and T. Ellenbogen, Nano Lett. **15**, 6215 (2015).
20. S. Balci and C. Kocabas, Opt. Lett. **40**, 3424 (2015).
21. R. Chikkaraddy, B. D. Nijs, F. Benz, S. J. Barrow, O. A. Scherman, E. Rosta, A. Demetriadou, P. Fox, O. Hess, and J. J. Baumberg, Nature **535**, 127 (2016).
22. S. Balci, B. Kucukoz, O. Balci, A. Karatay, C. Kocabas, and G. Yaglioglu, ACS Photon. **3**, 2010 (2016).
23. T. U. Tumkur, G. Zhu, and M. A. Noginov, Opt. Express **24**, 3921 (2016).
24. K. Zhang, W. B. Shi, D. Wang, Y. Xu, R. W. Peng, R. H. Fan, Q. J. Wang, and M. Wang, Appl. Phys. Lett. **108**, 193111 (2016).
25. A. Amo, T. C. H. Liew, C. Adrados, R. Houdre, E. Giacobino, A. V. Kavokin, and A. Bramati, Nat. Photonics **4**, 361 (2010).
26. C. Monroe, Nature **416**, 238 (2002).
27. D. Ballarini, M. D. Giorgi, E. Cancellieri, R. Houdre, E. Giacobino, R. Cingolani, A. Bramati, G. Gigli, and D. Sanvitto, Nat. Commun. **4**, 1778 (2013).
28. J. Kasprzak, M. Richard, S. Kundermann, A. Baas, P. Jeambrun, J. M. J. Keeling, F. M. Marchetti, M. H. Szymanska, R. Andre, J. L. Staehli, V. Savona, P. B. Littlewood, B. Deveaud, and L. S. Dang, Nature **443**, 409 (2006).
29. J. D. Plumhof, T. Stoferle, L. Mai, U. Scherf, and R. F. Mahrt, Nat. Mater. **13**, 247 (2014).
30. K. S. Daskalakis, S. A. Maier, R. Murray, and S. Kena-Cohen, Nat. Mater. **13**, 271 (2014).
31. S. Christopoulos, G. B. H. Hougersthal, A. J. D. Grundy, P. G. Lagoudakis, A. V. Kavokin, J. J. Baumberg, G. Christmann, R. Butte, E. Feltin, J. F. Carlin, and N. Grandjean, Phys. Rev. Lett. **98**, 126405 (2007).
32. S. Kena-Cohen and S. R. Forrest, Nat. Photonics **4**, 371 (2010).
33. L. C. Flatten, D. M. Coles, Z. He, D. G. Lidzey, R. A. Taylor, J. H. Warner, and J. M. Smith, Nat. Commun. **8**, 14097 (2017).
34. S. Dufferwiel, S. Schwarz, F. Withers, A. A. P. Trichet, F. Li, M. Sich, O. Del Pozo-Zamudio, C. Clark, A. Nalitov, D. D. Solnyshkov, G. Malpuech, K. S. Novoselov, J. M. Smith, M. S. Skolnick, D. N. Krizhanovskii, and A. I. Tartakovskii, Nat. Commun. **6**, 8579 (2015).
35. H. F. Ghaemi, T. Thio, D. E. Grupp, T. W. Ebbesen, and H. J. Lezec, Phys. Rev. B **58**, 6779 (1998).
36. Z. H. Tang, R. W. Peng, Z. Wang, X. Wu, Y. J. Bao, Q. J. Wang, Z. J. Zhang, W. H. Sun, and M. Wang, Phys. Rev. B **76**, 195405 (2007).
37. C. Billaudeau, S. Collin, C. Sauvan, N. Bardou, F. Pardo, and J. Pelouard, Opt. Lett. **33**, 165 (2008).